Tailoring a two-dimensional electron gas at the $LaAlO_3/SrTiO_3$ (001) interface by epitaxial strain

C. W. Bark[a], D. A. Felker[b], Y. Wang[c], Y. Zhang[d,e], H. W. Jang[a], C. M. Folkman[a], J. W. Park[a], S. H. Baek[a], H. Zhou[f], D. D. Fong[g], X. Q. Pan[d], E. Y. Tsymbal[c], M. S. Rzchowski[b], and C. B. Eom[a,1]

[a]Department of Materials Science and Engineering, University of Wisconsin, Madison, WI 53706; [b]Department of Physics, University of Wisconsin, Madison, WI 53706; [c]Department of Physics and Astronomy, Nebraska Center for Materials and Nanoscience, University of Nebraska, Lincoln, NE 68588; [d]Department of Materials Science and Engineering, University of Michigan, Ann Arbor, MI 48109; [e]National Laboratory of Solid State Microstructures and Department of Materials Science and Engineering, Nanjing University, Nanjing, 210093, People's Republic of China; [f]Chemical Sciences and Engineering Division, Argonne National Laboratory, Argonne, IL 60439; and [g]Materials Science Division, Argonne National Laboratory, Argonne, IL 60439

Edited* by T. H. Geballe, Stanford University, Stanford, CA, and approved January 12, 2011 (received for review October 11, 2010)

Recently a metallic state was discovered at the interface between insulating oxides, most notably $LaAlO_3$ and $SrTiO_3$. Properties of this two-dimensional electron gas (2DEG) have attracted significant interest due to its potential applications in nanoelectronics. Control over this carrier density and mobility of the 2DEG is essential for applications of these unique systems, and may be achieved by epitaxial strain. However, despite the rich nature of strain effects on oxide materials properties, such as ferroelectricity, magnetism, and superconductivity, the relationship between the strain and electrical properties of the 2DEG at the $LaAlO_3/SrTiO_3$ heterointerface remains largely unexplored. Here, we use different lattice constant single-crystal substrates to produce $LaAlO_3/SrTiO_3$ interfaces with controlled levels of biaxial epitaxial strain. We have found that tensile-strained $SrTiO_3$ destroys the conducting 2DEG, while compressively strained $SrTiO_3$ retains the 2DEG, but with a carrier concentration reduced in comparison to the unstrained $LaAlO_3/SrTiO_3$ interface. We have also found that the critical $LaAlO_3$ overlayer thickness for 2DEG formation increases with $SrTiO_3$ compressive strain. Our first-principles calculations suggest that a strain-induced electric polarization in the $SrTiO_3$ layer is responsible for this behavior. The polarization is directed away from the interface and hence creates a negative polarization charge opposing that of the polar $LaAlO_3$ layer. This behavior both increases the critical thickness of the $LaAlO_3$ layer, and reduces carrier concentration above the critical thickness, in agreement with our experimental results. Our findings suggest that epitaxial strain can be used to tailor 2DEGs properties of the $LaAlO_3/SrTiO_3$ heterointerface.

oxide interface | electronic transport | polar discontinuity

Strain has been used to engineer and enhance numerous properties of materials. For example, mobility in semiconductors (1,2), and transition temperatures in ferroelectric materials (3–6), and superconductors (7) have been controlled by strain. A recently discovered two-dimensional electron gas (2DEG) at the $LaAlO_3/SrTiO_3$ interface (8,9) has attracted great interest due to its unique application to nanoscale oxide devices (10). So far, most studies of 2DEGs at oxide interfaces were performed using TiO_2-terminated $SrTiO_3$ bulk single-crystal substrates. Despite the rich nature of strain effects on oxide materials properties, the relationship between the strain and electrical properties of the 2DEG at the $LaAlO_3/SrTiO_3$ heterointerface remains largely unexplored.

One important effect of strain arises from the constraint that integrating 2DEGs to other functional devices or substrates always involves strain. Understanding the effect of strain on a 2DEG at the $LaAlO_3/SrTiO_3$ interface is essential for these considerations. In addition, incorporation of strain might lead to unique functional properties. For example, strain can induce an electric polarization in otherwise nonpolar $SrTiO_3$ (11). It has been predicted that polarization can be used to control 2DEG properties at oxide heterointerfaces (12, 13). These effects provide tools to engineer the 2DEG behavior.

To address these issues, we explore the effect of epitaxial strain on transport properties of the $LaAlO_3/SrTiO_3$ interface. We create the 2DEG interface on strained single-crystal (001) $SrTiO_3$ templates grown on perovskite oxide substrates with various lattice mismatch. Pseudomorphic growth of the $LaAlO_3/SrTiO_3$ bilayer produces a continuously strained system, including the interface at which the 2DEG resides. This strained system allows us to add a new degree of freedom in the $LaAlO_3/SrTiO_3$ system and investigate the strain effect on its transport properties. We demonstrate that tensile strain makes the interface insulating, while compressive strain makes the interface metallic and allows modulating the critical thickness of $LaAlO_3$ and the 2DEG conductivity.

Experimental Methods

$LaAlO_3/SrTiO_3$ thin film heterostructures were grown on various single-crystal substrates using pulsed-laser deposition (PLD) with in situ high-pressure reflection high-energy electron diffraction (RHEED) (14). Fig. 1*A* shows the schematic of the thin film heterostructure. Table 1 shows substrates that were used in this study to vary the $SrTiO_3$ strain state from biaxial compressive to biaxial tensile in the plane. As shown in Fig. 1, (001) $SrTiO_3$ thin films were grown on (110) $NdGaO_3$ (NGO), (001) $(LaAlO_3)_{0.3} - (Sr_2AlTaO_6)_{0.7}$ (LSAT), (110) $DyScO_3$ (DSO), and (110) $GdScO_3$ (GSO) substrates. The varying lattice parameters result in an average biaxial strain ranging from −1.21% (compressive) to +1.59% (tensile) in a fully commensurate $SrTiO_3$ deposited film. All grown single-crystal (001) $SrTiO_3$ templates were fully coherent with the substrates. (001) $SrTiO_3$ films were also grown on (001) silicon (Si) substrates using Molecular Beam Epitaxy. Thickness of these quasi-single-crystal (001) $SrTiO_3$ templates on Si was 100 nm, and the films were almost fully relaxed. The measured $SrTiO_3$ lattice parameters on Si correspond to an average biaxial strain of 0.15% (15, 16). The biaxial strain state and lattice parameters of the strained (001) $SrTiO_3$ templates are summarized in Table 1. The full width at half maximum (FWHM) values of 002 rocking curves for the strained $SrTiO_3$ template are much narrower than that of the bulk $SrTiO_3$ single crystal (17). The single-crystal (001) $SrTiO_3$ templates were also etched using buffered hydrofluoric acid solution to maintain Ti-termination after the growth. The atomic percent of Sr, Ti, and O in the films were determined with wavelength dispersive X-ray spectroscopy. The chemical ratio of

Author contributions: C.W.B., M.S.R., and C.B.E. designed research; C.W.B., D.A.F., Y.W., Y.Z., H.W.J., C.M.F., J.W.P., S.H.B., H.Z., and D.D.F. performed research; C.W.B., D.A.F., Y.W., H.Z., D.D.F., X.Q.P., E.Y.T., and M.S.R. analyzed data; and C.W.B., D.A.F., E.Y.T., M.S.R., and C.B.E. wrote the paper.

The authors declare no conflict of interest.

*This Direct Submission article had a prearranged editor.

[1]To whom correspondence should be addressed. E-mail: eom@engr.wisc.edu.

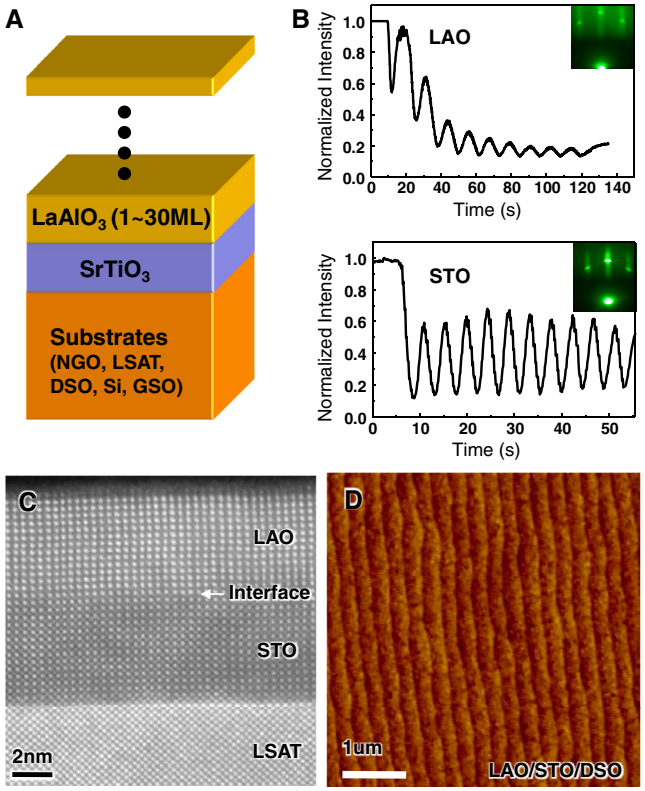

Fig. 1. Structural characterization of heterostructures. (*A*) Schematic diagram of grown structures. Thickness of $LaAlO_3$ layer was varied from 1 to 30 unit cells on STO on LSAT, NGO, Si, DSO, and GSO substrate, (*B*) RHEED intensity oscillations for the growth of LAO and STO on LSAT substrate. The insets show the RHEED pattern at the end of the LAO and STO growth. (*C*) High-resolution TEM image of LAO on STO on LSAT. Clear intensity differences between separate $LaAlO_3$ and $SrTiO_3$ layers in both cases and images showing distinctly the individual La and Sr atoms. (*D*) AFM images of LAO on STO on $DyScO_3$, substrates.

grown templates was the same as that of $SrTiO_3$ bulk single crystal within experimental error. This result confirms that the quality of $SrTiO_3$ templates is comparable with the bulk single-crystal $SrTiO_3$ substrate, ruling out extrinsic effects in our experiments.

$LaAlO_3$ overlayers were deposited using PLD on these variously strained Ti-terminated single-crystal $SrTiO_3$ templates. RHEED intensity oscillations of the specular spots show layer-by-layer growth mode (Fig. 1*B*), similar to those observed for $LaAlO_3$ films on $SrTiO_3$ single-crystal substrates. High-resolution transmission electron microscopy (TEM) cross-sectional image in Fig. 1*C* shows that the $LaAlO_3/SrTiO_3$ film on LSAT has high crystalline quality and an atomically sharp interface. For all substrates, surfaces of $LaAlO_3$ and $SrTiO_3$ films were atomically smooth with single unit cell high steps measured by atomic force microscopy (AFM), as seen in Fig. 1*D*. As a result, we confirmed that all biaxial strained heterostructures in this report were atomically controlled and grown epitaxially. More details about growth are described in ref. 11 and *Materials and Methods*.

Table 1. Results from high-resolution X-ray diffraction measurements on the films at room temperature are given

	a (Å)	c (Å)	Biaxial lattice mismatch
	$LaAlO_3$ *(10 uc) on* $SrTiO_3$ *(50 uc) on* $NdGaO_3$		
$SrTiO_3$	3.860	3.964	−1.21%
NGO	3.859	3.866	
	$LaAlO_3$ *(10 uc) on* $SrTiO_3$ *(100 uc) on LSAT*		
$SrTiO_3$	3.868	3.940	−0.96%
LSAT	3.869	3.867	
	$LaAlO_3$ *(10 uc) on* $SrTiO_3$ *(120 nm) on Si*		
$SrTiO_3$	3.911	3.985	0.15%
Si	3.840	3.840	
	$LaAlO_3$ *(10 uc) on* $SrTiO_3$ *(20 uc) on* $DyScO_3$		
$SrTiO_3$	3.944	3.939	1.11%
$DyScO_3$	3.944	3.939	
	$LaAlO_3$ *(10 uc) on* $SrTiO_3$ *(20 uc) on* $GdScO_3$		
$SrTiO_3$	3.964	3.875	1.59%
$GdScO_3$	3.963	3.967	

The in-plane (a) and out-of-plane (c) lattice constants and lattice mismatch between the $SrTiO_3$ films and single-crystal substrates on average of two orthogonal directions. The a- and c-lattice parameters of single-crystalline $SrTiO_3$ are 3.905 Å. All $SrTiO_3$ templates were fully coherent except STO/Si (12). (002), (101) of $SrTiO_3$ and cubic substrates, LSAT, Si $(200)_{pseudo\text{-}cubic}$ of $(101)_{pseudo\text{-}cubic}$ of orthorombic substrate, $GdScO_3$ and $DyScO_3$, $NdGdO_3$ were observed to determined in-plane and out-of-plane lattice parameters. Biaxial strain of $SrTiO_3$ templates

Results and Discussion

It is known experimentally that a conducting 2DEG forms at the $LaAlO_3$/bulk $SrTiO_3$ interface only after the $LaAlO_3$ overlayer thickness exceeds a critical value of four unit cells (18). We have found that this critical thickness depends on the strain of the system. We determined this critical thickness by measuring the conductivity of strained $LaAlO_3/SrTiO_3$ bilayers for different thickness of the $LaAlO_3$ layer. As shown in Fig. 1, the $LaAlO_3$ overlayer thickness was changed from 0 to 30 unit cells while the thickness of $SrTiO_3$ template on NGO, LSAT, DSO, and GSO substrates was fixed at 50 unit cells. We also checked the critical thickness of $LaAlO_3$ on Ti-terminated (001) $SrTiO_3$ bulk single crystal and on quasi-single-crystal (001) $SrTiO_3$ templates on Si (19) as a reference.

In the case of the two samples with unstrained $SrTiO_3$ layers ($LaAlO_3$ on bulk single-crystal $SrTiO_3$ substrate and $LaAlO_3$ on relaxed $SrTiO_3$ templates on Si), the critical thickness was in agreement with that previously reported, i.e., four unit cells. However, in the compressive strain states, ($SrTiO_3$ templates on LSAT and NGO), the critical thickness of $LaAlO_3$ increased to 10 unit cells and 15 unit cells, respectively, as shown in Fig. 2*A*. In all the cases, the conductivity saturated above the critical thickness of the $LaAlO_3$ overlayer. However, unlike the nonstrained state, the conductivity vs. thickness of $LaAlO_3$ had a gradual rather than an abrupt change at the critical thickness. For instance, in the case of $LaAlO_3/SrTiO_3$/LSAT measurable conductivity was detected at 10 unit cells (u.c.) $LaAlO_3$ thickness, but it did not saturate until 20 unit cells. There is however a clear trend of increasing $LaAlO_3$ critical thickness with increasing compressive biaxial in-plane strain.

Fig. 2*B* shows the room-temperature carrier concentration at each strain state above the critical thickness of $LaAlO_3$. Similar to the critical thickness of $LaAlO_3$ layer, we find nearly the same carrier concentration at both near-zero strain states, $LaAlO_3$ on $SrTiO_3$ bulk single crystal and $LaAlO_3$ on quasi-single crystal (001) $SrTiO_3$ template on Si. The saturation carrier concentration (above the critical thickness) decreased with increasing compressive strain. Although $LaAlO_3/SrTiO_3$ interfaces on DSO and GSO were grown and treated in the same manner, the interfaces were not conducting within our measurement limit at any thickness of $LaAlO_3$ overlayer in these tensile-strained films.

Our experimental results indicate that tensile-strained $SrTiO_3$ destroys the conducting interfacial 2DEG, while compressive-strained $SrTiO_3$ preserves the 2DEG, but with decreased interfacial carrier concentration. The maximum carrier concentration at the $SrTiO_3$ unstrained state suggests that it is the strain-dependence of $SrTiO_3$ properties that control the 2DEG. It has been predicted theoretically that free-standing biaxially strained $SrTiO_3$ under electrical short-circuit boundary conditions can develop an electric polarization (20, 21). Compressive strain is predicted to produce an [001] (out-of-plane) polarization, and

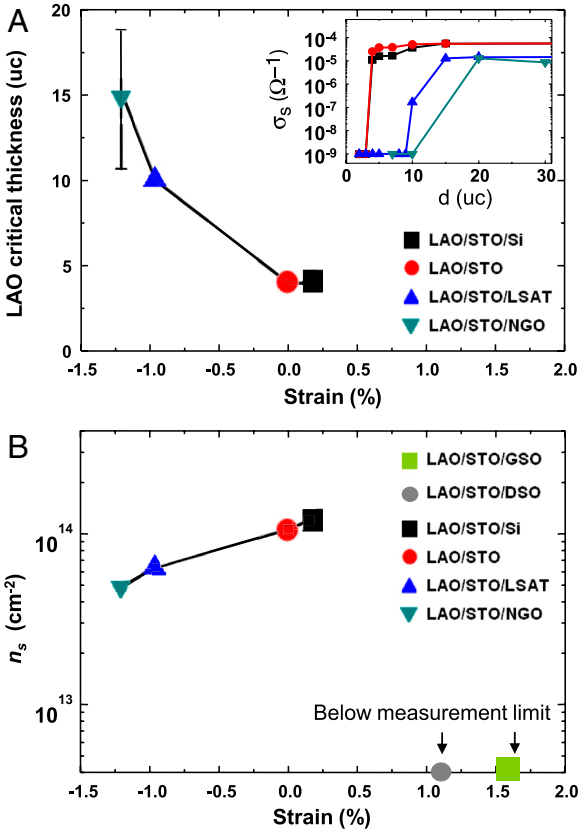

Fig. 2. Effect of strain on 2DEG. (*A*) Critical thickness of $LaAlO_3$ under biaxial strain. While other samples had 50 unit cell-thick $SrTiO_3$ layer, LAO/STO/Si had 100 nm-thick STO to get nominally unstrained STO layer on Si. Conductivity vs. thickness of $LaAlO_3$ in LAO/STO interface on various substrates was represented in inset. (*B*) Room-temperature carrier concentration at the LAO/STO interface under various biaxial strains. Carrier concentrations in tensile strain state were below our measurement limit.

tensile strain to produce a [110] (in-plane) polarization. Experimental evidence suggests a more complex picture, with many strain-states resulting in a relaxor behavior at room temperature (11, 22) without a stable switchable polarization.

However, we expect the strain-induced $SrTiO_3$ (STO) properties to be altered by the $LaAlO_3$ overlayer. Observations from TEM (23, 24), synchrotron radiation X-ray scattering (25, 26), and tunneling (27), indicate that in strain-free $SrTiO_3$ a few unit cells near the $LaAlO_3$ interface have ferroelectric-like structural distortions with local polarization pointing away from the interface, and decreasing in magnitude with distance from the interface (28). Biaxial compressive strain induces a tetragonal distortion along 001, which would enhance this polarization, potentially uniformly polarizing the $SrTiO_3$ throughout its thickness (29).

Fig. 3 schematically compares the strained and unstrained systems. In the unstrained system positively charged $(LaO)^+$ atomic layers and negatively charged $(AlO_2)^-$ atomic layers create an average polarization whose positive bound charge resides at the interface, as shown schematically in Fig. 3*A* (left). This polarization charge is responsible for the intrinsic electric field E_0 in $LaAlO_3$ (shown by arrow in Fig. 3*A*) resulting in an electric potential difference between the $LaAlO_3$ surface and the $LaAlO_3/SrTiO_3$ interface that increases with $LaAlO_3$ layer thickness. Above the $LaAlO_3$ critical thickness, charge is transferred to the $LaAlO_3/SrTiO_3$ interface (shown by a blue filling) to avoid this polarization catastrophe.

The compressively strained $SrTiO_3$ layer contains polar displacements of the Ti^{4+} ions with respect to the O^{2-} ions, shown in Fig. 3*B* for the case of uniform polarization. These displacements are responsible for a polarization P pointed away from the interface [indicated by an arrow at the bottom of Fig. 3*B* (left)]. The polarization orientation is determined by the presence of the $LaAlO_3$ layer and is likely not switchable. The polarization produces a negative bound charge at the $LaAlO_3/SrTiO_3$ interface [indicated in Fig. 3*B* (left)] that creates an additional electric field in $LaAlO_3$ equal to P/ε_{LAO}, where ε_{LAO} is the dielectric constant of $LaAlO_3$, that opposes the intrinsic electric field E_0. The presence of polarization in the compressively strained $SrTiO_3$ layer reduces the total electric field in $LaAlO_3$ and hence enhances the critical thickness necessary to create a 2DEG at the $LaAlO_3/SrTiO_3$ interface due to the polarization catastrophe effect. Above this critical thickness, the mobile interfacial carrier concentration would be reduced by the interfacial bound charge (12,13).

In order to quantify these effects we have completed first-principles calculations of the $LaAlO_3/SrTiO_3$ bilayer under various

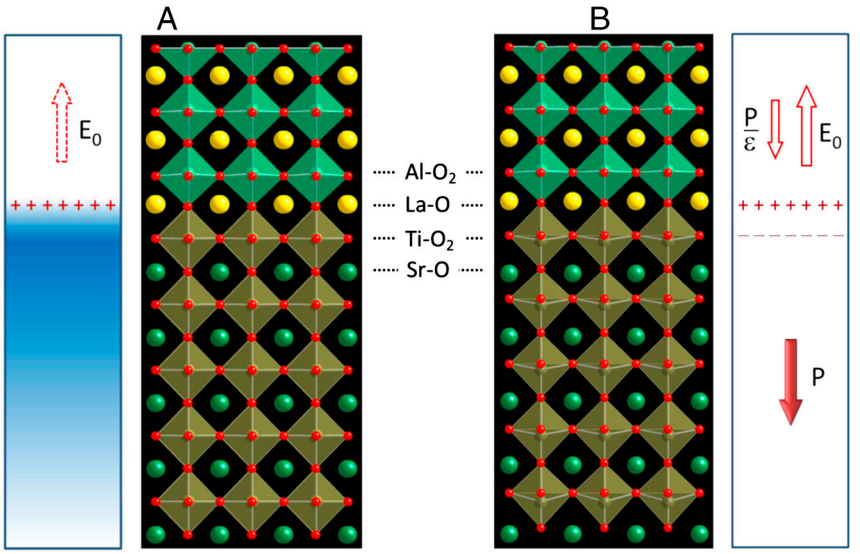

Fig. 3. Calculated atomic structure of unstrained (*A*) and compressively strained (*B*) $LaAlO_3$(3u.c.)/$SrTiO_3$ system. In *B* Ti-O and Sr-O displacements are amplified by a factor of eight as compared to the calculated results for visual comprehension. Left and right columns show schematically the 2DEG formation and the effect of the polarization P in the strained $SrTiO_3$ on the 2DEG as described in text.

strain states based on density functional theory (DFT), as described in *Materials and Methods*. Fig. 4 shows calculated ionic displacements for unstrained and 1.2% compressively strained $(LaAlO_3)_3/(SrTiO_3)_5$ structures. It is seen that in the unstrained case polar Ti-O displacements in the $SrTiO_3$ layer are very small, consistent with the previous calculations (30). The in-plane 1.2% compressive strain produces sizable ionic displacements, polarizing the $SrTiO_3$ layer. The calculation predicts that the induced polarization is oriented away from the interface and is not switchable. The magnitude of the polarization is $P \approx 0.18$ C/m^2, as found from the known polar displacements in the strained $SrTiO_3$ layer using the Berry phase method (31, 32).

The critical thickness t_c in the presence of a $SrTiO_3$ polarization can be estimated as follows:

$$t_c = \delta\boldsymbol{\varepsilon}/eE, \qquad [1]$$

where $\delta\boldsymbol{\varepsilon} = \boldsymbol{\varepsilon}_g + (\boldsymbol{\varepsilon}^{STO}_{VBM} - \boldsymbol{\varepsilon}^{LAO}_{VBM})$, $\boldsymbol{\varepsilon}_g$ is the band gap of $SrTiO_3$, $\boldsymbol{\varepsilon}^{STO}_{VBM}$ and $\boldsymbol{\varepsilon}^{LAO}_{VBM}$ are the valence band maxima (VBM) of $SrTiO_3$ and $LaAlO_3$ respectively, and E is the electric field in $LaAlO_3$. The latter is reduced from the intrinsic value of E_0 due to polarization P of $SrTiO_3$ so that

$$E = E_o - \frac{P}{\varepsilon_{LAO}}, \qquad [2]$$

where ε_{LAO} is the dielectric constant of $LaAlO_3$. Due to the reduced electric field in $LaAlO_3$ in the presence of the $SrTiO_3$ polarization, the critical thickness [**1**] is enhanced. The intrinsic electric field E_0 can be estimated from the experimentally measured critical thickness $t^0_c = 4$ u.c. for the unstrained system. Taking into account the experimental band gap of $SrTiO_3$ $\boldsymbol{\varepsilon}_g = 3.2$ eV and the VBM offset between $SrTiO_3$ and $LaAlO_3$ $\boldsymbol{\varepsilon}^{STO}_{VBM} - \boldsymbol{\varepsilon}^{LAO}_{VBM} = 0.35$ eV, (33) we find that $\delta\boldsymbol{\varepsilon} = 3.55$ eV. Using the relationship

$$\delta\boldsymbol{\varepsilon} = eE_o t^0_c \qquad [3]$$

we obtain that $E_0 \approx 0.23$ V/Å which is consistent with our first-principles calculation predicting $E_0 \approx 0.22$ V/Å, and with calculations by others (30, 34, 35). Using Eqs. **1**–**3** we obtain

$$t_c = \frac{t^0_c}{1 - \frac{P}{\varepsilon_{LAO}E_0}}. \qquad [4]$$

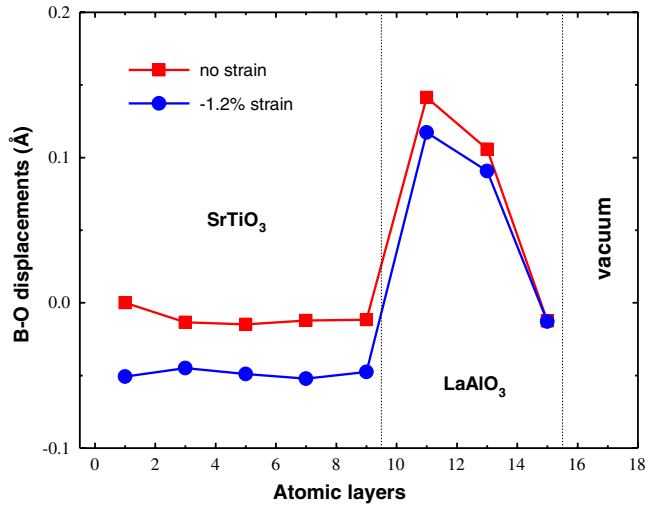

Fig. 4. B (Ti, Al) cite atom—oxygen (O) atom displacements in the unstrained (squares) and 1.2% compressively strained (circles) $(LaAlO_3)_3/(SrTiO_3)_5$ structure.

Using the calculated polarization value $P \approx 0.18$ C/m^2 for 1.2% compressive strain in the $SrTiO_3$ layer, and the calculated electric fields in the $LaAlO_3$ and $SrTiO_3$ layers in the strained $LaAlO_3/SrTiO_3$ system, we estimate the dielectric constant of the $LaAlO_3$ grown on 1.2% compressively strained $SrTiO_3$ to be $\varepsilon_{LAO} \approx 18\varepsilon_o$. This value is consistent with that obtained from the induced polarization of 0.34 C/m^2 in the $LaAlO_3$ layer, as is estimated from the calculated ionic displacements using the Berry phase method. [We note that the estimated value of the dielectric constant of the unstrained $LaAlO_3$ is $\varepsilon_{LAO} \approx 24\varepsilon_o$ which is consistent with the previously found result (36)]. Using. Eq. **4** and the dielectric constant $\varepsilon_{LAO} \approx 18\varepsilon_o$ we obtain $t_c \approx 9$ u.c.. This value is higher than the critical thickness (4 u.c.) for the unstrained system, and is consistent with the experimental result for the 1.2% strained $LaAlO_3/SrTiO_3$ structure. In the structural model used in our DFT calculation the $SrTiO_3$ polarization is screened by charge transferred to the $SrTiO_3$ surface.

For the case of tensile strain in the $SrTiO_3$ layer, our experiments indicate that there is no conducting 2DEG for biaxial tensile strains above 1.1%. Free-standing $SrTiO_3$ at zero temperature has been predicted to develop an in-plane polarization in the (110) direction under biaxial tensile strain. Experiment suggests that relaxor behavior, with nanoscale polar regions that can be aligned in an electric field, occurs in many tensile-strained $SrTiO_3$ samples at room temperature. Stabilization of a uniform in-plane polarization by the $LaAlO_3$ layer does not seem likely. If such nanoscale regions near to the interface were present in our samples, bound charge at polarization discontinuities between random nanopolar regions would tend to be locally screened by carriers at the 2DEG interface. This behavior would lead to localization of these carriers, preventing us from observing conduction in these samples.

Another aspect is strain in the $LaAlO_3$ overlayer. The bulk pseudocubic lattice constant of $LaAlO_3$ is 3.791 Å, so that coherent $LaAlO_3$ even on unstrained $SrTiO_3$ has a 3% tensile strain. Growing the bilayer on a GSO substrate results in 4.5% tensile strain in the $LaAlO_3$ layer. An NGO substrate reduces the $LaAlO_3$ strain to 1.8% tensile, but for all substrates used the $LaAlO_3$ layer is under tensile strain. Our TEM analysis of these samples indicates that the $LaAlO_3$ layer on $SrTiO_3$ is fully coherent when grown on LSAT (2% $LaAlO_3$ tensile strain) and $SrTiO_3$, but that growth on DSO (leading to 4% $LaAlO_3$ tensile strain) results in partial relaxation of the $LaAlO_3$. Such defect incorporation might alter the conduction properties of the interface. However, the $SrTiO_3$ layer on Si (grown by Molecular beam epitaxy) is almost fully relaxed, and the bilayer shows a fully conducting interfacial 2DEG, but with lower mobility. This observation suggests that such defects do not destroy the 2DEG. Large tensile strain in $LaAlO_3$ has been predicted (37) to alter the Al-O bond lengths, which could affect the electronic structure.

We have demonstrated that properties of the 2DEG formed at the $LaAlO_3/SrTiO_3$ interface can be controlled by epitaxial strain. Both the critical thickness of the $LaAlO_3$ overlayer required to generate the 2DEG and the carrier concentration of the 2DEG depend on the strain of the $SrTiO_3$ layer. Compressive strain increases the critical thickness and decreases the saturated carrier concentration. Our DFT calculations indicate that a strain-induced polarization stabilized by the $LaAlO_3$ overlayer is responsible for these changes. Changes in critical thickness and carrier concentration estimated from the DFT calculations are in agreement with the experimental data.

The dependence of 2DEG properties at the $LaAlO_3/SrTiO_3$ interface on the strain state opens a new correlation between strain-induced polarization and the electrical properties of oxide interfaces. We believe that such strain engineering can be very useful for oxide 2DEG device applications, and the relation between strain and 2DEG properties provides a new tool in the manipulation of oxide interfacial 2DEGs.

Materials and Methods

Epitaxial $LaAlO_3$ and $SrTiO_3$ thin films were grown on (001) LSAT, (110) $NdGaO_3$, (110) $GdScO_3$, and (110) $DyScO_3$ substrates by PLD. To grow heterostructures by PLD, substrates were attached to a resistive heater and positioned $5.0 \sim 6.0$ cm from the target. A KrF excimer laser (248 nm) beam was focused on a stoichiometric $LaAlO_3$ and $SrTiO_3$ single-crystal target to an energy density of $2.0 \sim 2.5$ J/cm^2 and pulsed at $3 \sim 5$ Hz. $SrTiO_3$ templates were grown at substrate temperatures ranging from 650 to 850 °C and oxygen pressures of 10–100 mTorr. Before deposition, low miscut (<0.05°) LSAT, NGO, DSO, and GSO substrates were treated by a modified buffered hydrofluoric acid etch and annealed in oxygen at $1{,}000 \sim 1{,}100$ °C for $2 \sim 12$ h to create atomically smooth surfaces with unit cell step. The PLD system is equipped with high-pressure RHEED, which enabled atomic layer controlled growth and in situ monitoring during the growth. $SrTiO_3$ templates were etched using buffered hydrofluoric acid for $30 \sim 90$ s to maintain Ti-termination after growth $SrTiO_3$ layer. $LaAlO_3$ films were grown at 550 °C at oxygen pressures of 10^{-3} mbar and cooled down to room temperature at the same oxygen pressure.

The three-dimensional strain state of the films was determined using high-resolution four-circle X-ray diffraction (Bruker D8 advance). The microstructure and interfacial structure of the samples were characterized by cross-sectional TEM. Film surfaces were imaged by AFM (Veeco).

After the growth, Al contacts were made by wire bonding near the four corners of the sample for van der Pauw electrical characterization. A Keithley 2700 sourcemeter combined with a 2400 switch matrix multimeter was used for the van der Pauw measurements of conductance and carrier concentration. The sheet resistance was calculated by fitting slopes to the four point IV curves measured between the four combinations of contacts. The nominal sheet carrier concentration was determined from the Hall coefficient as $n_{2D} = -t/R_H e$ where t is the film thickness, R_H is the Hall coefficient, and e is the charge of an electron. The mobility was determined from the sheet resistance $R_\square$ and sheet carrier concentration n_{2D} as $\mu = 1/en_{2D}R_\square$.

Density functional calculations were performed within the local density approximation using the plane-wave pseudopotential method (38, 39), similar to the calculations performed previously (40). In the calculations we neglected the effect of strong correlations which is justified due to both $LaAlO_3$ and $SrTiO_3$ being band insulators. We considered a LaO/TiO_2-interfaced $(LaAlO_3)_n/(SrTiO_3)_m$ bilayer (where n and m are the numbers of unit cells of $LaAlO_3$ and $SrTiO_3$ respectively), as a model system. The $LaAlO_3/SrTiO_3$ bilayer was placed in a $LaAlO_3/SrTiO_3$/vacuum/$SrTiO_3/LaAlO_3$/vacuum supercell, where the doubled bilayer was used to avoid an unphysical electric field in vacuum which otherwise would occur due to the potential step within the $LaAlO_3$ layer and periodic boundary conditions of the supercell calculations. The in-plane lattice constant of the unstrained superlattice was fixed to the calculated bulk lattice constant of $SrTiO_3$, i.e., $a = 3.871$ Å. For the strained systems the in-plane lattice constant was constrained to be a certain percentage smaller than the bulk one. To reduce the effect of the $SrTiO_3$ surface on atomic structure and ionic displacements within the $SrTiO_3$ layer we used a boundary condition according to which the atomic positions within one unit cell on the $SrTiO_3$ surface were fixed to be the same as in the respectively strained bulk $SrTiO_3$. The latter were computed separately for the unstrained and strained bulk $SrTiO_3$. All the other atoms in the superlattices were relaxed.

ACKNOWLEDGMENTS. This work was supported by the National Science Foundation (NSF) under Grant No. DMR-0906443, and a David and Lucile Packard Fellowship (C.B.E.). The work at University of Nebraska was supported by the Materials Research Science and Engineering Center (NSF Grant Number DMR-0820521), Experimental Program to Stimulate Competitive Research (NSF Grant Number EPS-1010674), and the Nebraska Research Initiative. The work at the University of Michigan was supported by DMR-0907191, DoE/BES DE-FG02-07ER46416, and NSF/DMR-0723032. Work at Argonne and use of the Advanced Photon Source were supported by the Department of Energy, Office of Science, Office of Basic Energy Sciences, under Contract No. DE-AC02-06CH11357.

1. Min C, Yongke S, Umamaheswari A, Thomas SE (2009) Strain: a solution for higher carrier mobility in nanoscale MOSFETs. *Annu Rev Mater Res* 39:203–229.
2. Welser J, Hoyt JL, Gibbons JF (1994) Electron mobility enhancement in strained-Si *n*-type metal-oxide-semiconductor field-effect transistors. *IEEE Electr Device L* 15:100–102.
3. Choi KJ, et al. (2004) Enhancement of ferroelectricity in strained $BaTiO_3$ thin films. *Science* 306:1005–1009.
4. Warusawithana MP, et al. (2009) A ferroelectric oxide made directly on Silicon. *Science* 324:367–370.
5. Reiner JW, et al. (2010) Crystalline oxides on Silicon. *Adv Mater* 22:2919–2938.
6. Woerdenweber R, Hollmann E, Kutzner R, Schubert J (2007) Induced ferroelectricity in strained epitaxial $SrTiO_3$ films on various substrates. *J Appl Phys* 102:044119-1–044119-5.
7. Gozar A, et al. (2008) High-temperature interface superconductivity between metallic and insulating copper oxides. *Nature* 455:782–785.
8. Ohtomo A, Hwang HY (2004) A high-mobility electron gas at the $LaAlO_3/SrTiO_3$ heterointerface. *Nature* 427:423–426.
9. Ohtomo A, Muller DA, Grazul JL, Hwang HY (2002) Artificial charge-modulation in atomic-scale perovskite titanate superlattices. *Nature* 419:378–380.
10. Cen C, Thiel S, Mannhart J, Levy J (2009) Oxide nanoelectronics on demand. *Science* 323:1026–1030.
11. Jang HW, et al. (2010) Ferroelectricity in strain-free $SrTiO_3$ thin films. *Phys Rev Lett* 104:169601-1–169601-4.
12. Niranjan MK, Wang Y, Jaswal SS, Tsymbal EY (2009) Prediction of a switchable two-dimensional electron gas at ferroelectric oxide interfaces. *Phys Rev Lett* 103:016804-1–016804-4.
13. Wang Y, Niranjan MK, Jaswal SS, Tsymbal EY (2009) First-principles studies of a two-dimensional electron gas at the interface in ferroelectric oxide heterostructures. *Phys Rev B* 80:165130-1–165130-10.
14. Rijnders GJHM, Koster G, Blank DHA, Rogalla H (1997) In situ monitoring during pulsed laser deposition of complex oxides using reflection high energy electron diffraction under high oxygen pressure. *Appl Phys Lett* 70:1888–1890.
15. Park JW, Baek SH, Bark CW, Biegalski MD, Eom CB (2009) Quasi-single-crystal (001) $SrTiO_3$ templates on Si. *Appl Phys Lett* 95:061902-1–061902-3.
16. Lee S, et al. (2010) Template engineering of Co-doped $BaFe_2As_2$ single-crystal thin films. *Nat Mater* 9:397–402.
17. Schlom DG, Chen L, Pan X, Schmehl A, Zurbuchen MA (2008) A thin film approach to engineering functionality into oxides. *J Am Ceram Soc* 91:2429–2454.
18. Thiel S, Hammerl G, Schmehl A, Schneider CW, Mannhart J (2006) Tunable quasi-two-dimensional electron gases in oxide heterostructures. *Science* 313:1942–1945.
19. Park JW, et al. (2010) Creation of a two-dimensional electron gas at an oxide interface on Silicon. *Nature Communications* 1:94 10.1038/ncomms1096.
20. Antons A, Neaton JB, Rabe KM, Vanderbilt D (2005) Tunability of the dielectric response of epitaxially strained $SrTiO_3$ from first principles. *Phys Rev B* 71:024102-1–024102-11.
21. Sheng G, et al. (2010) A modified Landau-Devonshire thermodynamic potential for strontium titanate. *Appl Phys Lett* 96:232902-1–232902-3.
22. Biegalski MD, et al. (2006) Relaxor ferroelectricity in strained epitaxial $SrTiO_3$ thin films on $DyScO_3$ substrates. *Appl Phys Lett* 88:192907-1–192907-3.
23. Maurice J, et al. (2006) Electronic conductivity and structural distortion at the interface between insulators $SrTiO_3$ and $LaAlO_3$. *Phys Status Solidi A* 203:2209–2214.
24. Jia CL, et al. (2009) Oxygen octahedron reconstruction in the $SrTiO_3/LaAlO_3$ heterointerfaces investigated using aberration-corrected ultrahigh-resolution transmission electron microscopy. *Phys Rev B* 79:081405-1–081405-4.
25. Vonk V, et al. (2007) Interface structure of $SrTiO_3/LaAlO_3$ at elevated temperatures studied in situ by synchrotron x rays. *Phys Rev B* 75:235417-1–235417-6.
26. Willmott PR, et al. (2007) Structural basis for the conducting interface between $LaAlO_3$ and $SrTiO_3$. *Phys Rev Lett* 99:155502-1–155502-4.
27. Singh-Bhalla G, et al. (2010) Built-in and induced polarization across $LaAlO_3/SrTiO_3$ heterojunctions. *Nature Physics*, 7 pp:80–86.
28. Haeni JH, et al. (2004) Room-temperature ferroelectricity in strained $SrTiO_3$. *Nature* 430:758–761.
29. Kamiya T, Kawasaki M (2008) ZnO-based semiconductors as building blocks for active devices. *MRS Bull* 33:1061–1066.
30. Pentcheva R, Pickett WE (2009) Avoiding the polarization catastrophe in $LaAlO_3$ overlayers on $SrTiO_3$ (001) through polar distortion. *Phys Rev Lett* 102:107602-1–107602-4.
31. Resta R (1992) Theory of the electric polarization in crystals. *Ferroelectrics* 136:51–55.
32. King-Smith RD, Vanderbilt D (1993) Theory of polarization of crystalline solids. *Phys Rev B* 47:1651–1654.
33. Segal Y, Ngai JH, Reiner JW, Walker FJ, Ahn CH (2009) X-ray photoemission studies of the metal-insulator transition in $LaAlO_3/SrTiO_3$ structures grown by molecular beam epitaxy. *Phys Rev B* 80:241107-1–241107-4.
34. Chen H, Kolpak AM, Ismail-Beigi S (2009) Fundamental asymmetry in interfacial electronic reconstruction between insulating oxides: an ab initio study. *Phys Rev B* 79:161402-1–161402-4.
35. Son W, Cho E, Lee B, Lee J, Han S (2009) Density and spatial distribution of charge carriers in the intrinsic *n*-type $LaAlO_3/SrTiO_3$ interface. *Phys Rev B* 79:245411-1–245411-7.
36. Lee J, Demkov AA (2008) Charge origin and localization at the *n*-type $SrTiO_3/LaAlO_3$ interface. *Phys Rev B* 78:193104-1–193104-4.
37. Hatt AJ, Spaldin NA (2010) Structural phases of strained $LaAlO_3$ driven by octahedral tilt instabilities. *Phys Rev B* 82:195402-1 195402-5.
38. Kresse G, Furthmüller J (1996) Efficient iterative schemes for ab initio total-energy calculations using a plane-wave basis set. *Phys Rev B* 54:11169 11186.
39. Kresse G, Furthmüller J (1996) Efficiency of ab-initio total energy calculations for metals and semiconductors using a plane-wave basis set. *Comp Mater Sci* 6:15–50.
40. Janicka K, Velev JP, Tsymbal EY (2009) Quantum nature of two-dimensional electron gas confinement at $LaAlO_3/SrTiO_3$ interfaces. *Phys Rev Lett* 102:106803-1–106803-4.